IAC-14.C1.1.3

INCORPORATING THE EVOLUTION OF MULTI-BODY ORBITS INTO THE TRAJECTORY TRADE SPACE AND DESIGN PROCESS

Amanda F. Haapala*
Purdue University, United States of America
ahaapala@purdue.edu

Kathleen C. Howell†
Purdue University, United States of America
howell@purdue.edu

David C. Folta‡
NASA Goddard Space Flight Center, United States of America
david.c.folta@nasa.gov

Libration point orbits have been incorporated in many missions, with the capability of orbiting near L_1 and L_2 in the Earth-Moon system recently demonstrated during the ARTEMIS mission. While the orbits in the vicinity of the collinear libration points have been well studied, knowledge about the availability and evolution of these orbits is not generally exploited during the mission design process. In this investigation, strategies to display information about the global solution space in the vicinity of the libration points are explored, facilitating a rapid assessment of the available solutions for a range of energy levels. A design process is presented that exploits information about the available orbit structures, and is demonstrated for several sample design scenarios, including transfers to and between libration point orbits.

Introduction

Within the last several decades, libration point orbits have been incorporated into many missions as, for example, the Sun-Earth L_1 and L_2 points prove quite useful for solar and cosmological observatories. The capability of excecuting a libration point mission in the Earth-Moon system was recently demonstrated during the ARTEMIS mission, where the impact of solar radiation in the lunar vicinity was examined as the Moon moved into and out of the Earth's magnetosphere. The orbits in the vicinity of the libration points have been well studied, providing a wealth of information about the available orbits and their evolution.[1–8] This information can be leveraged during the mission design process. For example, stability information associated with the GENESIS mission orbit was exploited to compute the invariant manifolds employed for the transfer design.[9] However, knowledge about the solution space is not generally exploited in current trajectory design tools. Collection and exploitation of this information within the design process would prove valuable to assess the available orbits against the design requirements, to consider possible trade-offs between the various orbit types, and to inform the selection of orbits that meet the mission constraints.

As mission requirements become increasingly complex, trajectory design tools that take advantage of the available natural dynamics are essential. Several tools exist that exploit dynamical systems theory for mission design, including Generator[10,11] and LTool.[12] A tool to interactively compute libration point orbits and their associated manifolds is demonstrated by Mondelo et al.[13] The AUTO software allows for computation of periodic orbits, numerical continuation of orbit families, as well as bifurcation detection and analysis.[14] An Adaptive Trajectory Design (ATD) strategy was demonstrated by Haapala et al., and provides interactive access to a variety of solutions for rapid design and analysis of trajectory options.[15] A dynamic reference catalog is introduced by Folta et al. as well as Guzzetti et al., and offers an interactive environment for orbit comparison and selection.[16,17]

In this investigation, strategies to display information about the global solution space in the vicinity of the libration points are explored, and their incorporation into the mission design process is demonstrated. Several distinct periodic and quasi-periodic orbit types are available in the vicinity of a libration point, and each may offer different advantages. As parameters, such as the Jacobi constant, change in value, the solution space evolves and the available orbits can be

*Ph.D. Candidate, School of Aeronautics and Astronautics
†Hsu Lo Distinguished Professor, School of Aeronautics and Astronautics
‡Senior Fellow, Aerospace Engineer

modified significantly. An overview of the current knowledge about this evolution is summarized, and a framework for the global solution space is charted, facilitating a rapid assessment of the available periodic and quasi-periodic solutions over a range of energy levels. A design process that exploits this information is demonstrated for several sample design scenarios.

Circular Restricted Three-Body Model

The Circular Restricted Three-Body (CR3B) problem[18] is a simplified model that offers insight about libration points and their associated orbits. In many cases, a preliminary design constructed within the framework of the CR3B can be transitioned to a higher-fidelity ephemeris model while maintaining the significant qualitative features of the original solution. In the Earth-Moon CR3B problem, the motion of a spacecraft, assumed massless, is determined by the gravitational forces of the Earth and the Moon, each represented as a point mass. The orbits of the Earth and Moon are assumed to be circular relative to the system barycenter. A barycentric rotating frame is defined such that the rotating x-axis is directed from the Earth to the Moon, the z-axis is parallel to the direction of the angular velocity of the primary system, and the y-axis completes the right-handed, orthonormal triad. The position of the spacecraft is defined relative to the Earth-Moon barycenter, and the six-dimensional state vector is written in terms of rotating coordinates as $\boldsymbol{x} = [x, y, z, \dot{x}, \dot{y}, \dot{z}]$. The mass parameter is defined as $\mu = \frac{m_2}{m_1+m_2}$, where m_1 and m_2 correspond to the mass of the Earth and Moon, respectively. The first-order, nondimensional, vector equation of motion is

$$\dot{\boldsymbol{x}} = \boldsymbol{f}(\boldsymbol{x}), \tag{1}$$

where the vector field, $\boldsymbol{f}(\boldsymbol{x})$, is defined

$$\boldsymbol{f}(\boldsymbol{x}) = \left[\dot{x}, \dot{y}, \dot{z}, 2n\dot{y} + U_x, -2n\dot{x} + U_y, U_z\right], \tag{2}$$

noting that the nondimensional mean motion of the primary system is $n = 1$. In Equations (1)-(2), $U(x, y, z, n) = \frac{1-\mu}{r_{13}} + \frac{\mu}{r_{23}} + \frac{1}{2}n^2\left(x^2 + y^2\right)$ is the pseudo-potential function, where the nondimensional Earth-spacecraft and Moon-spacecraft distances are written as r_{13} and r_{23}, respectively, and the quantities U_x, U_y, U_z represent partial derivatives of U with respect to rotating position coordinates. The only known integral of the motion is the Jacobi constant, evaluated as $C = 2U - v^2$, where $v = \left(\dot{x}^2 + \dot{y}^2 + \dot{z}^2\right)^{1/2}$. This quantity is a constant of the motion and offers useful information about the energy level associated with a given solution in the CR3BP.

Collinear Libration Points

The equations of motion described by equations (1)-(2) admit five equilibrium points, including three collinear points that lie along the x-axis, and two equilateral points. Linearization about any collinear libration point reveals an eigenvalue structure of the type saddle×center×center.[6,18,19] A pair of real roots, $\pm\sigma$, correspond to the one-dimensional stable and unstable manifolds. Two pairs of imaginary roots, $\pm i\nu$ and $\pm i\omega$, indicate that the center subspace is four-dimensional and oscillatory behavior exists in the vicinity of the libration point for the linear system. The eigenvalues $\pm i\nu$ correspond to oscillations in the $x - y$ plane, while the roots $\pm i\omega$ yield out-of-plane oscillations. Both periodic and quasi-periodic orbits exist and have been demonstrated to persist in the nonlinear model by a number of researchers.[5,7,8,20–22]

Periodic Orbits

Lyapunov and Vertical Orbits

From a linear analysis, the existence of Lyapunov and vertical orbits is demonstrated. Employing an orbit from the linear system as the initial guess, a periodic orbit may be constructed in the nonlinear model using a differential corrections or targeting algorithm. From the converged solution in the nonlinear model, families comprised of the Lyapunov and vertical orbits are computed via numerical continuation.[8] Thus, solutions within the global center manifold associated with a libration point are located. Sample members from the families of Lyapunov and vertical orbits appear for the Earth-Moon system in Figs. 1 and 2. All families in Figs. 1 and 2 emerge directly from the libration point with the two fundamental frequencies ν and ω. The orbits within the families are colored consistent with the associated value of Jacobi constant so that red→blue corresponds to higher→lower values of Jacobi constant. Note that the color mapping is not the same among the different families.

Stability of Periodic Orbits

In addition to the families of Lyapunov and vertical orbits, as computed in the nonlinear system, families of halo and axial orbits also exist. These families bifurcate from the Lyapunov and vertical orbit families, that is, the originating member of the halo family is also a member of the planar Lyapunov family, and two 'originating' members of the axial family exist and are also members of the Lyapunov and vertical families. To locate bifurcations, the stability of the orbits within the families is examined.

To explore the stability of a periodic orbit, it is useful to first examine the linear variational equations. Consider the linear system $\delta\dot{\boldsymbol{x}} = \boldsymbol{A}(t)\delta\boldsymbol{x}$, where $\delta\boldsymbol{x} = \boldsymbol{x} - \boldsymbol{x}_r$, $\boldsymbol{x}_r$ is some reference solution, $\boldsymbol{A}(t) = D\boldsymbol{f}(\boldsymbol{x}_r)$ is the Jacobian matrix of first partial derivatives of $\boldsymbol{f}$, and $\boldsymbol{f}$ is defined as in equation (2) for the CR3BP. The general solution to the linear equations of motion is of the form $\delta\boldsymbol{x}(t) = e^{\boldsymbol{A}(t-t_0)}\delta\boldsymbol{x}(t_0)$, and the state transition matrix (STM) is defined as $\boldsymbol{\Phi}(t, t_0) = e^{\boldsymbol{A}(t-t_0)}$,

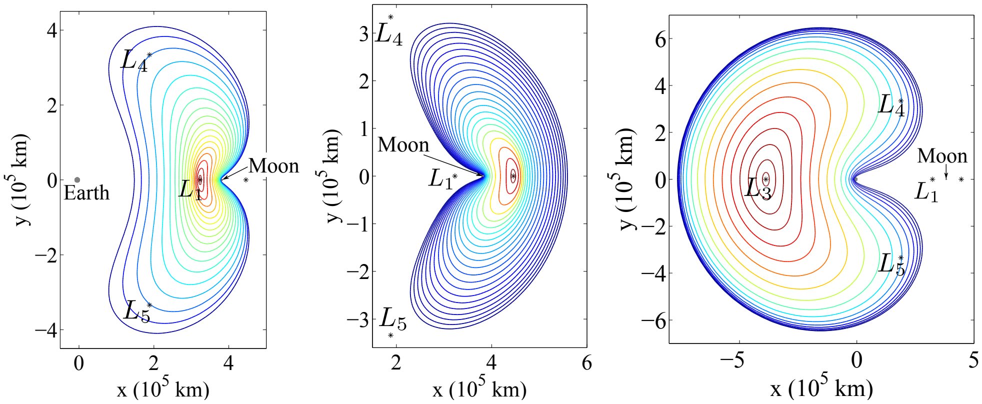

a) L_1 family **b)** L_2 family **c)** L_3 family

Fig. 1 Sample members from the families of Lyapunov and vertical orbits in the Earth-Moon system; Jacobi constant denoted by color

where $\boldsymbol{A}$ is not constant, in general.

Define $\boldsymbol{\Gamma}(t)$ as the set of all states along a periodic orbit of period T; then $\boldsymbol{x}^* = \boldsymbol{\Gamma}(\tau)$, $0 \leq \tau \leq T$, serves as a fixed point along $\boldsymbol{\Gamma}(t)$. A stroboscopic mapping is defined by the monodromy matrix $\boldsymbol{\Phi}(T, 0)$, i.e., the STM computed by integrating the state associated with the fixed point for one period of the orbit. The monodromy matrix possesses eigenvalues λ_i that occur in reciprocal pairs, and the associated eigenvectors, $\boldsymbol{v}_i$, span $\mathbb{R}^n$. Thus, the space is defined by the union of three invariant subspaces, E_S, E_U, and E_C. Let n_S be the number of eigenvalues with real parts of magnitude < 1, n_U be the number with real parts of magnitude > 1, and n_C be the number for which $|\lambda| = 1$, so that $n = n_S + n_U + n_C = \text{rank}(\boldsymbol{\Phi}(T, 0))$. Then, the dimensions of the invariant subspaces E_S, E_U, and E_C are n_S, n_U, and n_C, respectively. The monodromy matrix possesses at least one pair of unit eigenvalues whose associated eigenvectors are tangent to the periodic solution at the fixed point, thus, $n_C \geq 2$ always. If $n_C \geq 4$, a nontrivial center manifold is predicted from linear analysis. For a linearly stable periodic orbit, $n_C = 6$ and stable and unstable manifolds associated with the periodic solution may not exist in the nonlinear system. For unstable periodic orbits, at least one reciprocal pair of real eigenvalues $\lambda_U = \frac{1}{\lambda_S}$ exists such that $|\lambda_U| > 1$ and stable/unstable manifolds associated with the fixed point exist. Because a periodic solution is defined by an infinite number of fixed points along the orbit, the stable/unstable manifolds are composed of an infinite number of asymptotic trajectories.

Halo and Axial Orbits

Stepping along the families of Lyapunov and vertical orbits in Figs. 1 and 2, parameters such as the orbital period, Jacobi constant value, and the orbital stability, defined in terms of λ_i, evolve continuously. The location at which a stability change occurs within a family of periodic orbits is denoted as a bifurcation point. Different types of stability changes are possible, and the type determines any qualitative changes that exist as a result of the bifurcation. By tracking the changes in stability along a particular family of orbits, bifurcations to other distinct orbit families are located. For the Lyapunov and vertical families of orbits, plots depicting the stability of individual orbits within each family appear in Figs. 3-5. For each representative orbit from Figs. 1 and 2, the number of eigenvalue pairs for which $|\lambda| = 1/|\lambda| = 1$ is recorded, not including the trivial pair of unit eigenvalues that exist for any periodic orbit. When $(n_C - 2)/2 = 0$, the orbit is unstable with stable and unstable subspaces of dimension $n_S = n_U = 2$, and there exists no center manifold except for that associated with the pair of unit eigenvalues. If $(n_C - 2)/2 = 1$, $n_S = n_U = 1$ and a nontrivial center subspace of dimension $n_C - 2 = 2$ is predicted from the linear analysis. Orbits corresponding to $(n_C - 2)/2 = 2$ are linearly stable, i.e., are associated with a nontrivial center subspace of dimension $n_C - 2 = 4$ and may not possess stable or unstable manifolds in the nonlinear system.

Examining the evolution of the orbital stability across the Lyapunov and vertical families, several bifurcations exist and are summarized in Table 1. The first bifurcation, Ly-1, in each of the Lyapunov families yields the families of halo orbits. The northern halo families are plotted for the Earth-Moon system in Fig. 6. Southern families are computed by reflecting the northern families across the $x$$-$$y$ plane. The second bifurcation, Ly-2, signals the emergence of the families of axial orbits from the plane. Portions of the axial families appear in Fig. 7. Only those orbits for which $z > 0$ at the maximal value of y are plotted. The second half of the families are computed by reflecting these members across the $x - y$ plane. Again, the individual orbits within the families in Figs. 6-7 are colored according to the associated value of Jacobi constant, however, the color mapping is not consistent across the different families. The L_1 and L_2 Lyapunov families

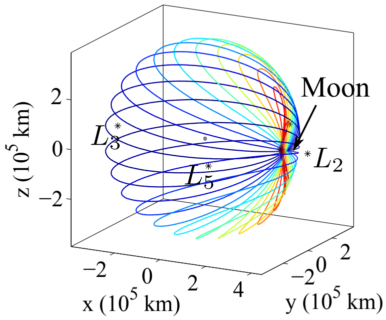

a) L_1 family

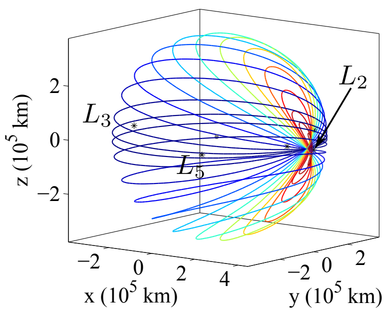

b) L_2 family

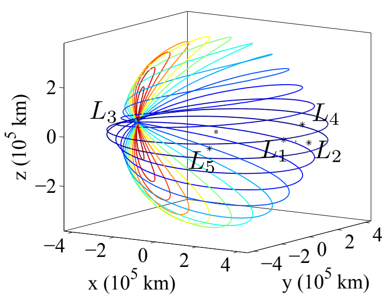

c) L_3 family

Fig. 2 Sample members from the families of vertical orbits in the Earth-Moon system; Jacobi constant denoted by color

possess a third bifurcation, Ly-3, which corresponds to a period-doubling bifurcation. The third bifurcation, Ly-4, in the L_3 Lyapunov family connects to families of planar orbits that originate from the equilateral points, L_4 and L_5.[8] From examination of the stability plots for the vertical families, several additional bifurcations are apparent. The first bifurcation in each family is labeled V-1, and corresponds to a bifurcation to the respective axial families. The bifurcation, V-2, corresponds to a period-doubling bifurcation from a family of planar orbits.[21] The L_3 vertical family connects to the L_4 and L_5 families of vertical orbits via the bifurcation V-3.[8]

Plots representing the stability corresponding to the halo orbits appear in Fig. 8. For the halo families, the number of complex eigenvalue pairs is represented as a function of orbit amplitude ratio A_z/A_y. At the points H-1, H-2 and H-4, the L_1 and L_2 families experience period-doubling bifurcations. A stability change occurs in the family at H-3 and H-5, but does not lead

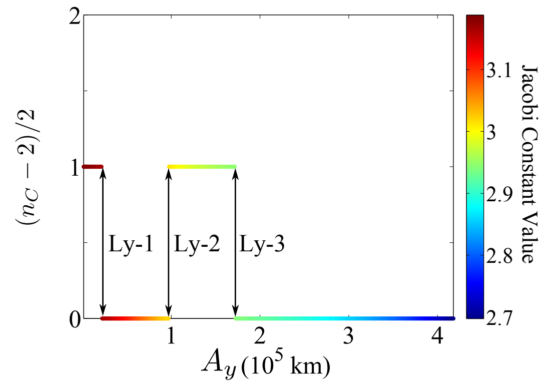

a) L_1 Lyapunov family

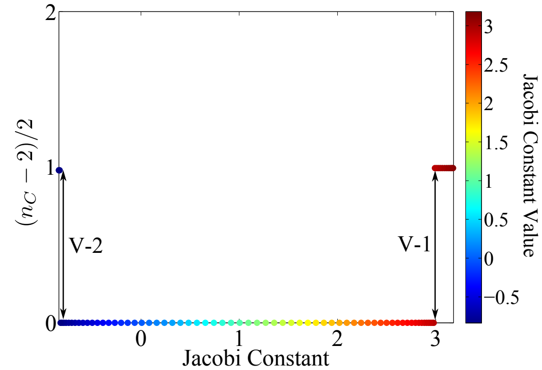

b) L_1 vertical family

Fig. 3 Stability information for Lyapunov and vertical orbits in the Earth-Moon system; Jacobi constant denoted by color

to any new orbit families.[5] The L_2 halo family undergoes a period-doubling bifurcation, H-6, that yields the family of L_2 butterfly orbits.[8] Only those orbits with perilune above the surface of the Moon are included in the plots, thus, a bifurcation from the L_1 family of halo orbits to the L_4 and L_5 families of axials orbits does not appear in the L_1 halo stability chart.[8] The axial orbits are unstable ($n_c = 2$) for each of the families.

Table 1 Bifurcations in Periodic Orbit Families

Label	Bifurcation
Ly-1	halo family
Ly-2	axial family
Ly-3	period-doubling
Ly-4	planar L_4,L_5 families
V-1	axial family
V-2	‘reverse’ period-doubling
V-3	L_4 and L_5 vertical families
H-1, H-2, H-4, H-6	period-doubling
H-3, H-5	cyclic fold

Quasi-Periodic Orbits

For a periodic orbit possessing a nontrivial center manifold, nearby quasi-periodic solutions exist.

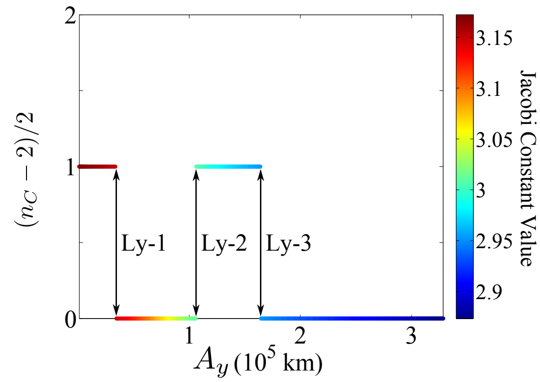

a) L_2 Lyapunov family

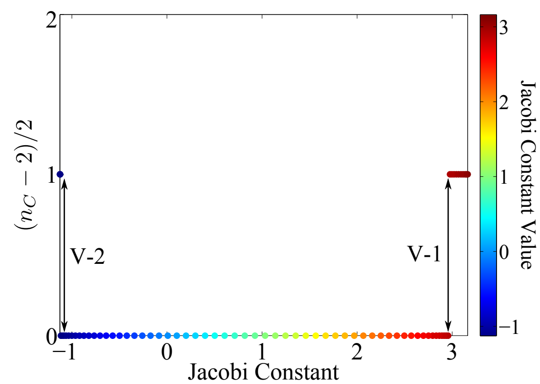

b) L_2 vertical family

Fig. 4 Stability information for Lyapunov and vertical orbits in the Earth-Moon system; Jacobi constant denoted by color

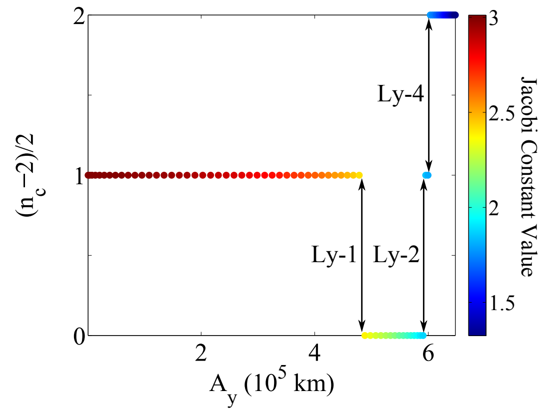

a) L_3 Lyapunov family

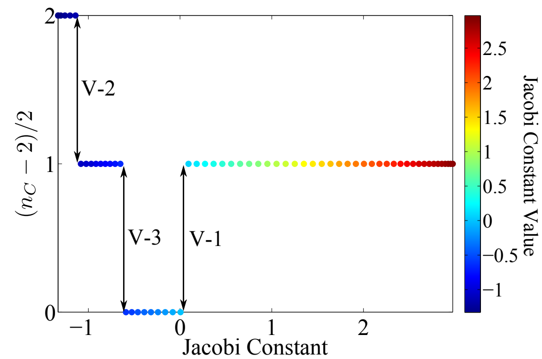

b) L_3 vertical family

Fig. 5 Stability information for Lyapunov and vertical orbits in the Earth-Moon system; Jacobi constant denoted by color

These orbits are bounded, and close only as $t \to \infty$, that is, they are periodic solutions with infinite period. The path traced by a quasi-periodic orbit lies on the surface of an invariant torus of dimension two or greater. Thus, a quasi-periodic orbit is defined by two or more frequencies, in contrast to the single frequency associated with a periodic orbit. Quasi-periodic orbits have been computed previously by various researchers.[22–24] In this investigation, the tori are computed directly via methods demonstrated by Olikara and Scheeres.[25] Note that a similar strategy is demonstrated by Castellá and Jorba and employed by Gómez and Mondelo.[7,23] Assuming the function $\boldsymbol{\psi}(\theta_0, \theta_1)$ describes a two-dimensional torus on which a quasi-periodic orbit lies with associated frequencies $\omega_0 = \dot{\theta}_0$, $\omega_1 = \dot{\theta}_1$, then, the dimension may be reduced to one by selecting an initial value of θ_0 so that an invariant circle, $\boldsymbol{u}(\theta_1)$, along the torus is defined. Integrating some initial state $\boldsymbol{u}(\theta_1 = \theta_{1,0})$ along this circle for time $T_q = \frac{2\pi}{\omega_0}$ yields the final state on the circle $\boldsymbol{u}(\theta_{1,0} + \rho_q)$, where $\rho_q = \omega_1 \cdot T_q$. A map, $\boldsymbol{G}$, is defined based on the frequencies ω_0, ω_1 so that propagating discretized states along $\boldsymbol{u}(\theta_1)$ for time T_q and removing the rotation by the angle ρ_q yields $\boldsymbol{G}(\boldsymbol{u}) = \boldsymbol{u}$. To compute a torus, a differential corrections algorithm is employed to determine the values for T_q, ρ_q, and the discretized states along $\boldsymbol{u}(\theta_1)$ that satisfy $\boldsymbol{G}(\boldsymbol{u}) - \boldsymbol{u} = \boldsymbol{0}$, while applying an additional constraint on the value of Jacobi constant. Once a torus is constructed, pseudo-arclength continuation is employed to locate additional tori in the family, assuming that additional phase constraints on θ_0 and θ_1 are incorporated. Gaps in a family of tori may occur due to resonance in the torus frequencies. Pseudo-arclength continuation is successful to generate the complete family of tori as long as these resonance gaps are not too large. Given a periodic orbit, a family of tori is initialized by employing the associated stability information to locate a linear approximation for a nearby invariant circle. Let $\lambda_C = e^{i\rho}$ be a complex eigenvalue and $\boldsymbol{v}_C$ a corresponding eigenvector associated with the monodromy matrix computed from a fixed point $\boldsymbol{x}^*$ along the periodic orbit. Then, the initial guess for an invariant curve centered on $\boldsymbol{x}^*$ is of the form $\boldsymbol{u}(\theta_1) = k \cdot (\cos(\theta_1)\mathrm{Re}(\boldsymbol{v}_C) - \sin(\theta_1)\mathrm{Im}(\boldsymbol{v}_C))$, where k is a small value used to scale the circle. The period T and the argument ρ of the complex eigenvalue associated with the central periodic orbit serve as an initial guess for the values of T_q and ρ_q associated with a nearby torus. A truncated Fourier series is used to represent the invariant curve, and a Newton-

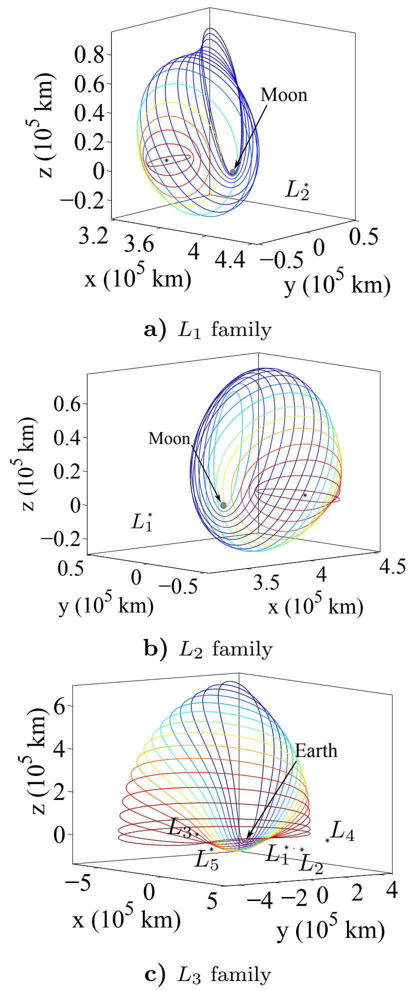

a) L_1 family

b) L_2 family

c) L_3 family

Fig. 6 Sample members from the families of halo orbits in the Earth-Moon system; Jacobi constant denoted by color

Raphson method is employed to compute T_q, ρ_q, and the discretized states along $\boldsymbol{u}(\theta_1)$ that satisfy the constraints. Further details on the computation of tori are available in Olikara and Scheeres.[25]

For a periodic orbit with a nontrivial center manifold of dimension $(n_C - 2)/2 \geq 1$, quasi-periodic orbits associated with the central periodic orbit may be computed via the previously described approach. For example, a halo orbit that exists for a Jacobi constant value greater than that of the bifurcation H-1 in the L_1 and L_2 halo families corresponds to $n_C = 4$ and there exists a family of quasi-periodic solutions identified as the quasi-halo orbits in the vicinity of the halo orbits. All L_3 halo orbits appearing in Fig. 6 correspond to $n_C = 4$. Selecting the L_1 halo orbit corresponding to $C = 3.15$, sample members from the family of quasi-halo tori, each also corresponding to the Jacobi constant value $C = 3.15$, are computed and appear in Fig. 9 as gray surfaces. A different quasi-halo orbit covers the surface of each of these two-dimensional tori; note that, while the orbits and tori may appear to be self-intersecting when projected into configuration

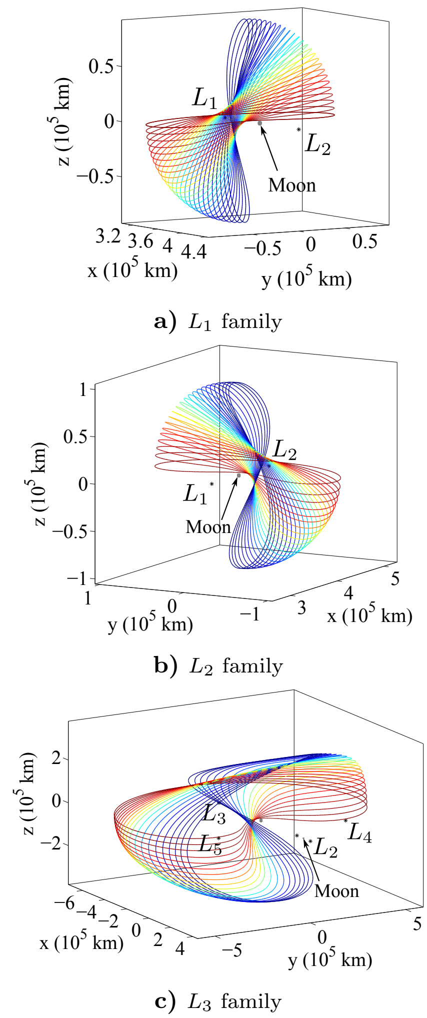

a) L_1 family

b) L_2 family

c) L_3 family

Fig. 7 Sample members from the families of axial orbits in the Earth-Moon system; Jacobi constant denoted by color

space, they do not self-intersect in the full phase space. Similarly, an orbit that exists before the bifurcation V-1 in the families of L_1, L_2 and L_3 vertical orbits in Fig. 2 corresponds to $n_C = 4$, and there exists a family of quasi-vertical orbits, commonly labeled the Lissajous orbits, in the vicinity of each of these vertical orbits. Sample tori associated with the L_2 vertical orbit that exists for $C = 3.15$ appear in Fig. 10, and a different Lissajous orbit covers the surface each torus. For energies less than (higher Jacobi constant values than) the bifurcating orbit at V-1, this family of tori offers a bridge between the Lyapunov and vertical orbits, and can be computed using either periodic orbit to initiate the family. Thus, the tori collapse to the planar orbit as they evolve away from the vertical orbit.

Libration Point Orbit Evolution and Frequency Analysis

Examining the frequencies associated with periodic libration point orbits is useful to demonstrate the relationships between the orbit families. The Lyapunov and vertical families of orbits inherit their orbital pe-

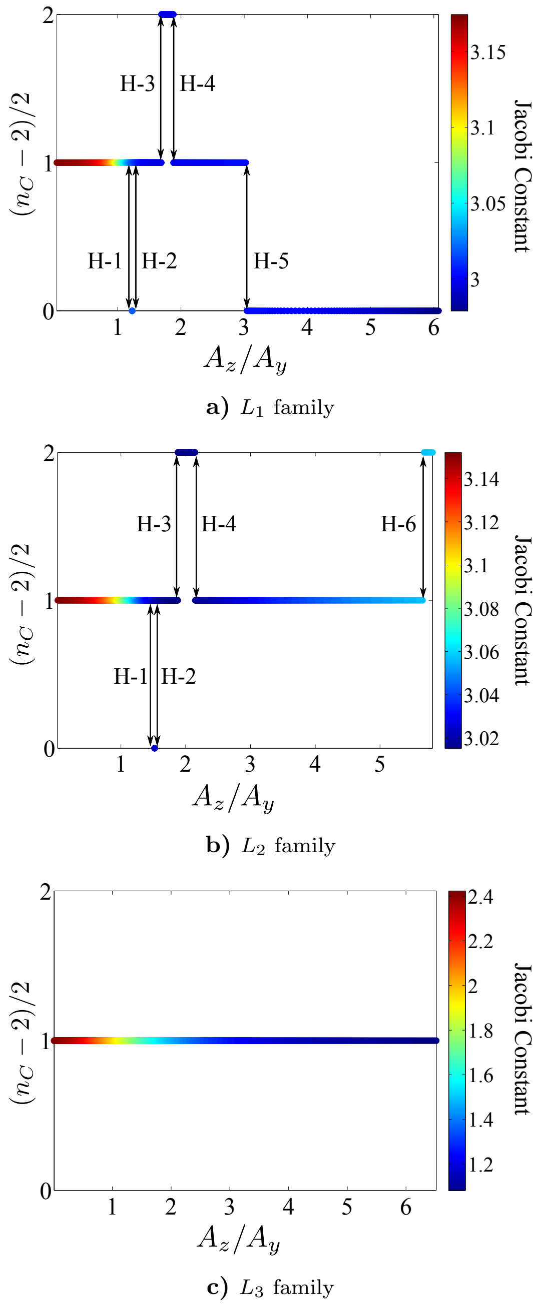

Fig. 8 Stability information for halo orbits in the Earth-Moon system

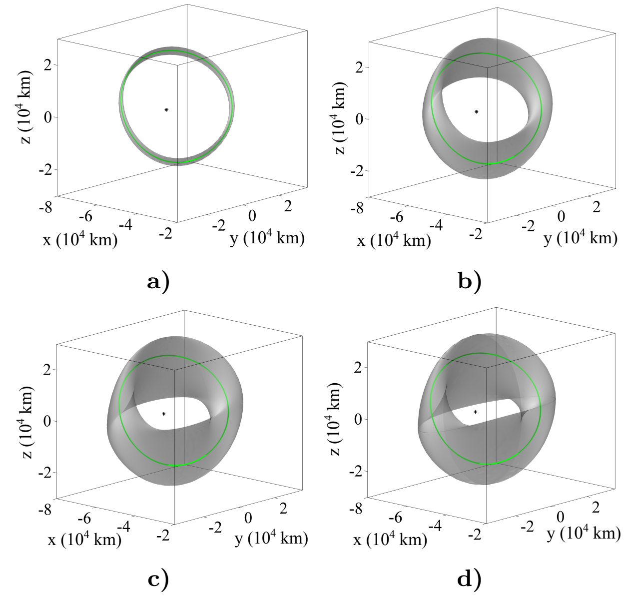

Fig. 9 L_1 quasi-halo tori in the Earth-Moon system for $C = 3.15$

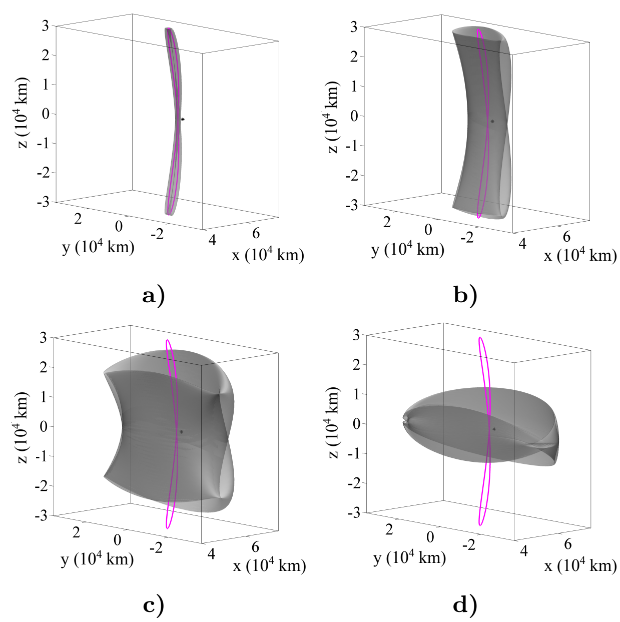

Fig. 10 L_2 Lissajous tori in the Earth-Moon system for $C = 3.15$

riods from the two central frequencies associated with the collinear point. The Lyapunov orbit family originates from the 'planar' frequency ν associated with the libration point, while the vertical orbits inherit the 'vertical' frequency ω, as demonstrated by the blue and magenta curves in Fig. 11. In the figure, the halo orbit family bifurcates from the L_1 Lyapunov orbits, as indicated by the green line that branches from the blue Lyapunov curve. The families of axial orbits bifurcate from both the Lyapunov and vertical orbits, thus, the cyan axial line bridges the blue and magenta arcs.

For energy levels less than (higher Jacobi constant values than) that associated with the bifurcation Lyapunov 1 to the halo family, both the Lyapunov and vertical orbits possess a nontrivial center subspace of dimension $n_C - 2 = 2$. Using the approach from Olikara and Scheeres to compute tori, the families of quasi-Lyapunov and quasi-vertical tori are constructed for $C = 3.18$. The frequencies ω_0 and ω_1 associated with the quasi-periodic orbits appear in Fig. 12(a). Because the family of tori bridges the Lyapunov and vertical orbits, the quasi-Lyapunov and quasi-vertical orbits form a single black curve in the figure. Define T_L and ρ_L as the period and the argument of the complex eigenvalue, respectively, associated with the Lyapunov orbit, and T_v and ρ_v as the period and the argument

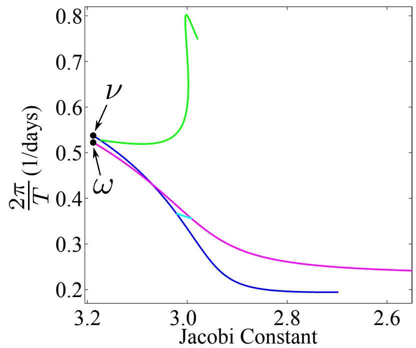

Fig. 11 Frequencies associated with L_1 Lyapunov (blue), vertical (magenta), halo (green), and axial (cyan) orbits

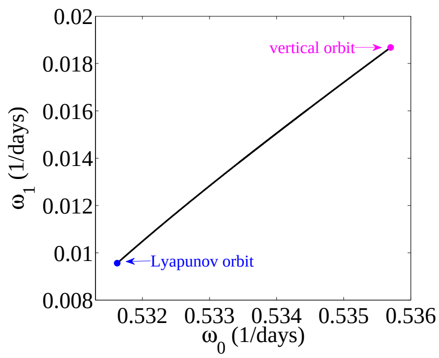

a) $C = 3.18$

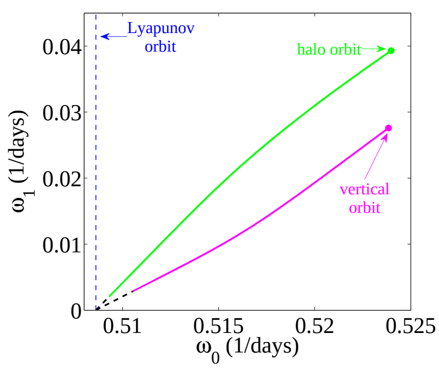

b) $C = 3.15$

Fig. 12 Frequency analysis for L_1 orbits

of the complex eigenvalue associated with the vertical orbit. The frequencies associated with the periodic orbits are additionally plotted, where $\omega_0 = 2\pi/T_L$, $\omega_1 = \rho_L/T_L$ for the Lyapunov and $\omega_0 = (2\pi + \rho_v)/T_v$, $\omega_1 = \rho_v/T_v$ for the vertical orbit. Note the addition of the angle ρ_v in the expression for ω_0 for the vertical orbit; this is included to define ω_0 so that it represents the frequency of in-plane oscillations as a torus collapses to the plane. The periodic Lyapunov (blue) and vertical (magenta) orbits for $C = 3.18$ are depicted in Fig. 13(a). The Poincaré map defined by crossings of the hyperplane $\Sigma = \{\boldsymbol{x} | z = 0\}$ is computed for sample quasi-Lyapunov/quasi-vertical orbits. Map crossings are projected into configuration space and plotted in gray in the figure. As the crossings of

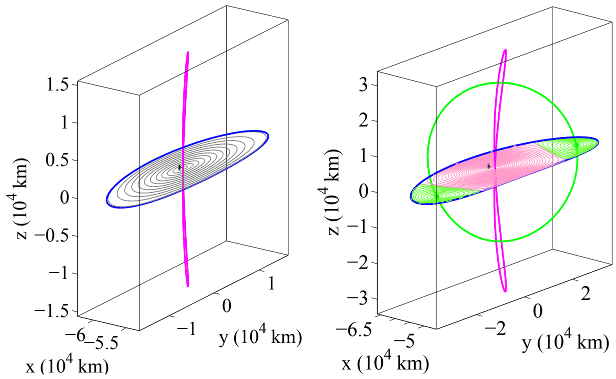

a) $C = 3.18$ **b)** $C = 3.15$

Fig. 13 Poincaré maps representing L_1 orbits

the map approach the Lyapunov orbit, the associated torus collapses to the plane.

After the bifurcation Ly-1 to the halo families, the northern and southern halo orbits emerge and the Lyapunov orbit loses its nontrivial center manifold. Thus, the quasi-Lyapunov orbits do not exist between the Jacobi constant values associated with the bifurcations Ly-1 and Ly-2. Families of quasi-halo and quasi-vertical orbits are computed for $C = 3.15$ and the associated frequencies are represented in Fig. 12(b). Clearly, each family originates from the frequencies of the associated central periodic orbit. As the quasi-periodic orbits evolve along the family, their frequencies approach that associated with the Lyapunov orbit, $\omega_0 = \frac{2\pi}{T_L}$, indicated by the blue dashed line. Note that the black dashed lines represent a linear interpolation between the last computed tori in the families and $\omega_0 = 2\pi/T_L$, $\omega_1 = 0$. The Lyapunov, vertical, and halo (green) orbits for $C = 3.15$ appear in Fig. 13(b), in addition to the projection of the $z = 0$ Poincaré map crossings for sample quasi-halo and quasi-vertical orbits. From the freqency plot and Poincaré map it is clear that the quasi-halo and quasi-vertical orbits form two distinct families.

Continuing to evolve the energy level beyond the bifurcation Ly-2 to the axial family, the Lyapunov orbit regains a nontrivial center manifold and a new family of quasi-Lyapunov orbits emerges. A Poincaré map representing selected L_1 orbits, including the Lyapunov, vertical, halo, and axial (cyan) map crossings, appears for $C = 3.01$ in Fig. 14(a). For this energy level, the periodic Lyapunov, vertical, and halo orbits have each passed through a number of period multiplying bifurcations. Thus, additional periodic orbits exist and their crossings may be added to the Poincaré map. The family of quasi-halo orbits (green) is interrupted by a period-2 (p-2) halo orbit for which $n_C = 4$. The crossings of this p-2 halo orbit appear in orange, in addition to the p-2 quasi-halo region. A second p-2 halo orbit also exists, corresponding to $n_C = 2$, and

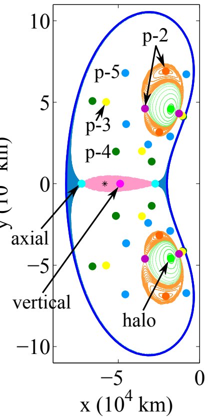

a) Poincaré map

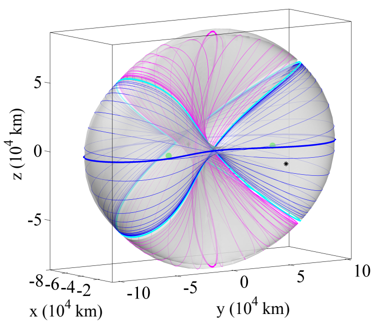

b) Sample tori

Fig. 14 Sample L_1 orbits for $C = 3.01$

crossings of this orbit are included in purple. In addition, crossings along p-3, p-4, and p-5 halo orbits are represented in yellow, dark green, and light blue, and many more period-multiple halo orbits may be computed for this value of Jacobi constant. (Note that one pair of the dark green crossings is nearly covered by the yellow crossings of the p-3 halo in the figure.) The quasi-Lyapunov orbit crossings are computed and are plotted on the map in blue. This family evolves from orbits with nearly planar oscillations to a torus with relatively large z-excursions that are bounded by the cyan axial orbits; a sample torus appears in gray in Fig. 14(b) with a 150-day propagation of an orbit on the surface included in blue. Sample quasi-vertical orbit crossings are represented on the map in pink, with a torus plotted in gray in Fig. 14(b) in addition to a 130-day propagation of the orbit in magenta.

Stable and Unstable Manifolds

For any periodic orbit, $\boldsymbol{\Gamma}(t)$, with $n_S = n_U > 1$, stable and unstable manifolds exist and provide asymptotic flow into and out of the orbit. A local stable/unstable manifold is computed by introducing a perturbation in some state, $\boldsymbol{x}^* = \boldsymbol{\Gamma}(\tau)$, $0 \leq \tau \leq T$, along the periodic orbit in the direction of the stable/unstable eigenvector associated with the monodromy matrix, $\boldsymbol{\Phi}(\tau + T, \tau)$, corresponding to $\boldsymbol{x}^*$. Assume that $\lambda^S < 1$ and $\lambda_U = 1/\lambda_S$ are stable and unstable eigenvalues of the monodromy matrix associated with a periodic orbit. Let $\boldsymbol{w}^U$ and $\boldsymbol{w}^S$ be their associated eigenvectors, and define $\boldsymbol{w}^{U+}$, $\boldsymbol{w}^{U-}$, $\boldsymbol{w}^{S+}$, $\boldsymbol{w}^{S-}$ as the two directions associated with each eigenvector. The local half-manifold, $W^{U-}_{\boldsymbol{x}^*,loc}$ ($W^{S-}_{\boldsymbol{x}^*,loc}$), is approximated by introducing a perturbation relative to $\boldsymbol{x}^*$ along the periodic orbit in the direction $\boldsymbol{w}^{U-}$ ($\boldsymbol{w}^{S-}$). Likewise, a perturbation relative to $\boldsymbol{x}^*$ in the direction $\boldsymbol{w}^{U+}$ ($\boldsymbol{w}^{S+}$) produces the local half-manifold $W^{U+}_{\boldsymbol{x}^*,loc}$ ($W^{S+}_{\boldsymbol{x}^*,loc}$). The magnitude of the step along the direction of the eigenvector is denoted d, and the initial states along the local stable manifolds are computed as $\boldsymbol{x}^{S+} = \boldsymbol{x}^* + d \cdot \boldsymbol{w}^{S+}$, $\boldsymbol{x}^{S-} = \boldsymbol{x}^* - d \cdot \boldsymbol{w}^{S-}$, where $\boldsymbol{w}^{S+}$ and $\boldsymbol{w}^{S-}$ are normalized so that the vector containing the position components of the eigenvector is of unit length; this normalization provides a physical meaning for the value of d as a distance. The local stable/unstable manifolds are globalized by propagating the states $\boldsymbol{x}^{S+}$ ($\boldsymbol{x}^{S-}$)/$\boldsymbol{x}^{U+}$ ($\boldsymbol{x}^{U-}$) in reverse-time/forward-time in the nonlinear model. This process yields the numerical approximation for the global stable manifolds, $W^{S+}_{\boldsymbol{x}^*}$ ($W^{S-}_{\boldsymbol{x}^*}$), and unstable manifolds, $W^{U+}_{\boldsymbol{x}^*}$ ($W^{U-}_{\boldsymbol{x}^*}$). The value of d is critical because it determines the accuracy with which the global manifolds are approximated. Selecting d too small yields manifold trajectories that require long integration times before departure from the vicinity of the periodic orbit, leading to accumulation of numerical error. If d is too large, then the approximation to the local manifold is poor. Here, a value of $d = 20$ km is selected so that propagating the initial state along the manifold back toward the periodic orbit, i.e., propagating $\boldsymbol{x}^{S-}, \boldsymbol{x}^{S+}$ in forward-time and $\boldsymbol{x}^{U-}, \boldsymbol{x}^{U+}$ in reverse-time, yields a manifold trajectory that remains in the vicinity of the periodic orbit for at least two revolutions. The collection of all unstable manifolds forms the surfaces W^{U+} and W^{U-} that reflect asymptotic flow away from the periodic orbit. Likewise, the collection of all stable manifolds forms the surfaces W^{S+} and W^{S-} that reflect asymptotic flow toward the orbit. In Fig. 15(a), a subset of trajectories on the unstable/stable manifold associated with an L_1 northern halo/L_2 vertical orbit in the Earth-Moon system are propagated for a fixed time interval, and are plotted in red/blue.

Several numerical schemes have been developed to locate the stable/unstable manifolds asymptotic to quasi-periodic orbits.[19,26] In this analysis, families of quasi-periodic tori and their associated manifolds are computed numerically using techniques demonstrated by Olikara and Scheeres.[25] Recalling that a periodic orbit represents a fixed point under the stroboscopic map $\boldsymbol{F}(\boldsymbol{x})$ defined by time T, then stability information for the periodic orbit is recovered by examining the eigenvalues of the linearization of the map, i.e., the monodromy matrix $\boldsymbol{\Phi}(T, 0) = \boldsymbol{F}_{\boldsymbol{x}}$. Analogously, the invariant circle, $\boldsymbol{u}(\theta_1)$, represents a fixed point of the map $\boldsymbol{G}(\boldsymbol{u})$ defined by frequencies ω_0 and ω_1. Thus, stability of the torus is determined by the eigenvalues of the matrix $\boldsymbol{G}_{\boldsymbol{x}}$, i.e., the linearization of the map $\boldsymbol{G}$; the eigenvectors corresponding to eigenvalues that lie off of the unit circle in the complex plane provide the directions tangent to the stable and unstable manifolds associated with each of the discretized states along $\boldsymbol{u}(\theta_1)$ on the torus. More details on the computation of quasi-periodic tori and their associated manifolds are available in Olikara and Scheeres.[25] Examples of tori corresponding to quasi-halo (left) and Lissajous (right) orbits appear in Fig. 15(b). For each torus, a single manifold trajectory is propagated for a fixed time interval; propagating the manifolds back toward the quasi-periodic orbits (in forward-/reverse-time for the stable/unstable manifold) for $2 \cdot T_q$ yields the two revolutions along the quasi-periodic orbits in black.

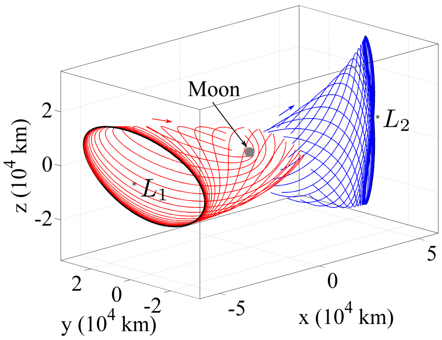

a)

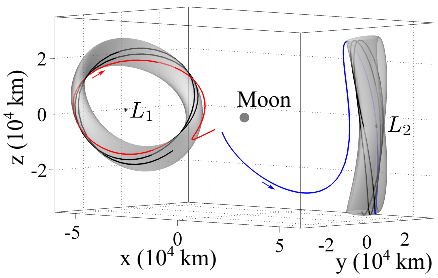

b)

Fig. 15 Sample stable (blue) and unstable (red) manifolds associated with libration point orbits in the Earth-Moon system for $C = 3.15$

Incorporating Orbit Evolution into the Design Process

In the previous sections, a review of the evolution of the libration point orbits is offered. Methods of consolidating this information into charts that can be employed within the mission design process would prove useful in selecting orbits that best meet mission requirements. For example, knowledge about the evolution of periodic orbit stability with Jacobi constant value is useful to determine the existence of periodic orbits as well as their associated stable/unstable and center manifold structures. The stability information from Figs. 3-5, and 8 is collected to produce the chart in Fig. 16. Here the orbit family names appear in the boxed labels, and the bifurcations from Table 1 are included as well. Members from the various periodic orbit families are represented by their associated value of Jacobi constant, and are colored according to the dimension of the unstable subspace $n_U = n_S$ such that $n_U = 2 \rightarrow$ red, $n_U = 1 \rightarrow$ green, and $n_U = 0 \rightarrow$ blue. In the chart, the abscissa is inverted so that moving along the horizontal axis corresponds to increasing energy (decreasing Jacobi constant). Note that the vertical families extend beyond the limits of the chart, thus, not all orbits in the family appear in the plot. Also, the L_3 families of halo and axial orbits exist for a range of Jacobi constant values that does not appear within the axis limits on this chart. For the L_1 and L_2 halo families, more than one orbit may exist for a particular value of C. In such cases, multiple lines appear on the chart to represent the family, where one line above another indicates a higher value of the amplitude ratio A_z/A_y, and A_y and A_z represent the maximal $y-$ and $z-$excursions along an orbit. For example, two L_2 halo orbits exist between the values $C = 3.015 - 3.059$; for this range of C, the orbits with a higher value of A_z/A_y appear as a second line above the first. So that the orbit families for each of the collinear points are clearly represented in one chart, the vertical axis in Fig. 16 serves only to differentiate between the orbit families. To include additional information, such as orbit amplitudes, it is useful to consider a reduced set of orbits for clarity. For example, the plot in Fig. 17 represents orbit amplitude information for the Earth-Moon L_2 Lyapunov, vertical, halo, and axial orbits for a range of Jacobi constant values. The horizontal blue and orange dashed lines, and vertical black dashed lines are included for an upcoming example.

Additional information, such as representative transfer costs, could also be included in the analysis. Folta, Bosanac, Guzzetti, and Howell implement an interactive approach to compare transfer and stationkeeping costs, among other parameters, across various orbit types.[16,17] Folta et al. compute the cost to transfer to Lyapunov, halo, quasi-halo, vertical, and Lissajous orbits for a variety of Jacobi constant values, assuming a direct transfer from a 200 km low-Earth orbit (LEO) to a libration point orbit, achieved by performing one tangential maneuver (Δv_1) at LEO, and one maneuver (Δv_2) at the x-axis crossing of the libration point orbit where $\dot{y} < 0$.[27] Varying the energy level of the orbit impacts the cost of direct transfer significantly, where cost is defined as the magnitude of Δv_2 for locally optimal transfers. Generally, the cost for direct transfers decreases with Jacobi constant for the halo and Lyapunov orbits. For two orbits at the same value of C, the cost is less for that maneuver possessing the smaller z-amplitude at insertion on the libration point orbit. Many other transfer types exist and could be included in the analysis. For example, transfers to halo orbits employing stable manifolds have been computed by Parker and Born;[28] Folta et al. additionally demonstrated a reduction in cost achieved by including a maneuver near the Moon, where, the cost to insert into an L_2 halo orbit decreases with A_z.[27]

Informing the Orbit Selection Process

Including charts that supply information about the global solution space in the vicinity of the collinear

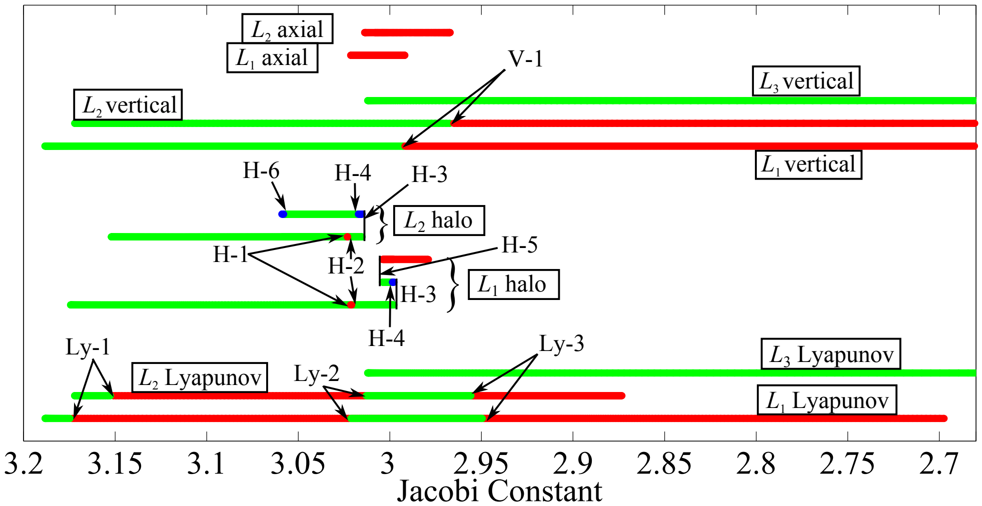

Fig. 16 Evolution of stability for L_1 and L_2 orbit families; $(n_C - 2)/2 = 0$ (red), 1 (green), 2 (blue)

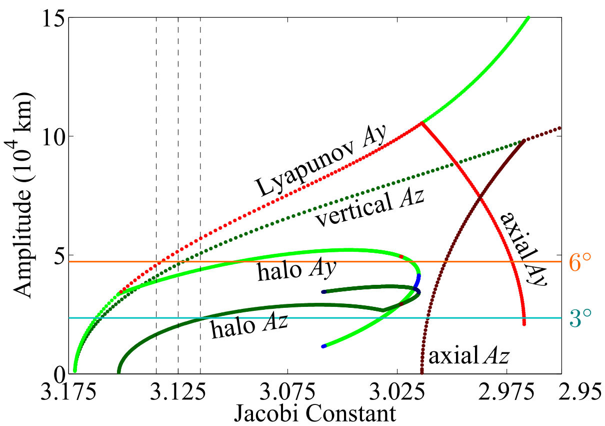

Fig. 17 Amplitude and stability information for L_2 Lyapunov, vertical, halo, and axial orbits.

points within the mission design process allows mission designers to exploit the currently available information, and improves the efficiency of the design process. The charts in Figs. 16 and 17 are useful to:

- determine the existence of specific orbit types at various energies and amplitudes
- approximate quasi-periodic orbit amplitude ranges
- locate orbits with stable/unstable manifolds
- locate orbits with a possible center manifold

For example, if it is desirable to transfer onto an L_1 quasi-halo orbit via the stable manifold, the Jacobi constant values corresponding to the green portions of the L_1 halo lines in Fig. 16 should be considered since, for these orbits, the linear analysis predicts the existence of a center manifold and indicates that stable/unstable manifolds are available. In addition to revealing information about the available manifold structures, Fig. 17 offers periodic orbit amplitude information, which also proves useful to gain insight about the amplitude ranges associated with the families of quasi-periodic orbits in the vicinity of the libration point for a given energy level.

Design Examples

Transfer to an L_1 Lissajous Orbit

Because many of the vertical and Lissajous orbits involve significant time intervals above/below the ecliptic plane, they are useful to avoid interference from zodiacal light. However, a direct transfer to an L_1 vertical orbit requires at least 100 m/s more Δv when compared with transfers to L_1 halo orbits.[27] If longer transfer times are an option, it is often more efficient in terms of propellant to incorporate a lunar pass into the transfer. Thus, it may be desirable to initially transfer to an L_2 orbit of low A_z and construct a connection between the L_2 halo and L_1 vertical orbits. From Fig. 17 it is apparent that lower L_2 halo orbit z-amplitudes generally correspond to higher values of Jacobi constant, thus, it is useful to explore energy levels near the bifurcating orbit from the L_2 Lyapunov family ($C = 3.152$). To compute the connection between the L_2 and L_1 orbits, it is necessary to select an energy level for which the orbits possess stable and unstable manifolds. Additionally, the Lissajous orbits exist only for vertical orbits corresponding to $n_C \geq 4$. Thus, the green ranges of the L_1 vertical orbits in Fig. 16, and green or red ranges along the L_2 halo orbit bar are considered.

To design the transfer, the northern and southern L_2 halo orbits and the L_1 vertical and family of quasi-vertical orbits are computed for $C = 3.14$. For this energy level, the L_1 vertical orbit is unstable with a nontrivial center manifold, and the cost of a direct transfer to a quasi-vertical orbit is estimated to lie within the range 550-715 m/s from the charts that appear in Folta et al.[27] The unstable manifold associated with each of the halo orbits is approximated using 1000 trajectories computed as previously described. The stable manifold surfaces asymptotic to each of the quasi-vertical orbits are generated via the method of Olikara and Scheeres.[25] Each manifold arc is numerically integrated for 15 nondimensional time units (65 days, forward-time for unstable, reverse-time for stable), and crossings of the surface of section $\Sigma = \{\boldsymbol{x} | x = 1 - \mu\}$ are recorded. The resulting Poincaré map is four-dimensional; the map is projected onto the $y - z$ plane in Fig. 18(a), where blue points represent the quasi-vertical stable manifold trajectories, and red crossings represent the unstable manifold arcs that depart the northern and southern halo orbits. To search for a

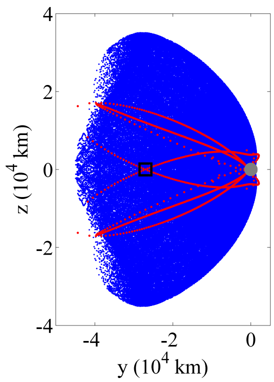

a) $y - z$ projection for Σ

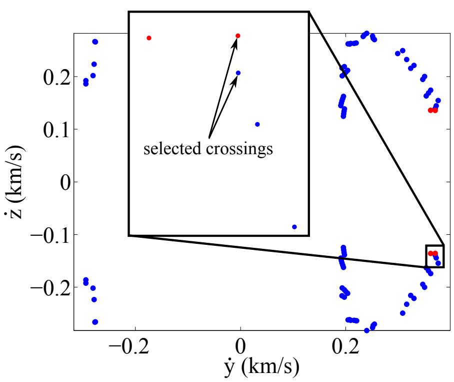

b) $\dot{y} - \dot{z}$ projection for Σ_*

Fig. 18 Transfer to an L_1 quasi-vertical orbit in the Earth-Moon system for $C = 3.14$

heteroclinic connection, the method demonstrated by Goméz et al.[29] is employed: the dimension of the map is reduced by selecting values y_*, z_* and a new surface of section $\Sigma_* = \{\boldsymbol{x} | x = 1 - \mu, y = y_*, z = z_*\}$ is defined. Because only a finite number of manifold arcs are propagated, all points within the boundaries $y_* - \delta y \le y \le y_* + \delta y$, $z_* - \delta z \le z \le z_* + \delta z$ are considered, where $\delta y = \delta z = 578.5$ km for this example. The small black box in Fig. 18(a) is centered on the selected coordinates y_*, z_*, however, the dimensions of this box are exaggerated compared to the selected values of δy, δz. Examining only those points within the prescribed tolerance of the surface Σ_*, the projection of the resulting two-dimensional Poincaré map onto the $\dot{y} - \dot{z}$ plane appears in Fig. 18(b). Selecting the red and blue points that are closest on the map, i.e., those within the black box in Fig. 18(b), and propagating the corresponding manifold arcs, an initial guess for a heteroclinic connection between the L_2 southern halo orbit and an L_1 quasi-vertical torus is generated and appears in Fig. 19(a). Here, a discontinuity exists where the red and blue arcs meet. (Note that Poincaré maps for $C = 3.15$ indicate that a

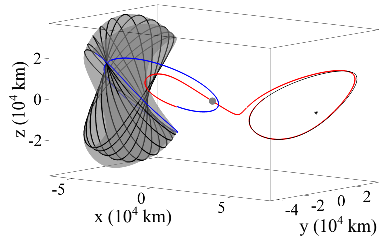

a) Initial guess

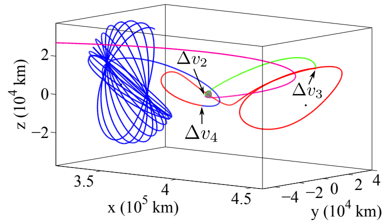

b) Corrected transfer near Moon

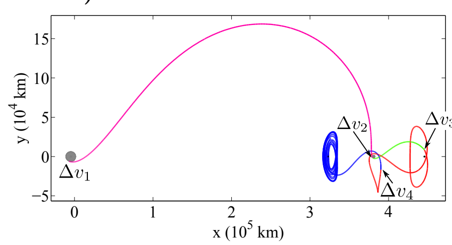

c) Corrected transfer

Fig. 19 Transfer to an L_1 quasi-vertical orbit in the Earth-Moon system

heteroclinic connection does not exist for this precise energy level).

Before a corrections process is applied, the initial guess is modified to include: 1) an Earth conic arc to provide the transfer arc from LEO to the Moon, 2) a lunar conic arc to allow transfer from the Moon to the initial state along the halo orbit unstable manifold. The modified trajectory is, then, corrected in a Sun-Earth-Moon ephemeris model. Departure with a tangential maneuver (Δv_1) is enforced from a 200 km LEO of 28.5° inclination. The location of the second maneuver is constrained to a 200 km altitude perilune passage. The third and fourth maneuvers to insert onto the Lissajous orbit stable manifold are not constrained, except that $\Delta v_2 + \Delta v_3 + \Delta v_4$ is reduced to less than 300 m/s via a continuation method. The maneuvers are as follows: $\Delta v_1 = 3.134$ km/s, $\Delta v_2 = 181.8$ m/s, $\Delta v_3 = 100.9$ m/s, $\Delta v_4 = 16.2$ m/s. The time-of-flight along the corrected path is 172.6 days, where the magenta and green transfer arcs require 5.7 and 3.0 days, respectively, and the red arc corresponds to a 23.5 day time-of-flight. The final Lissajous orbit is associated with a Jacobi constant value near $C = 3.147$.

Modifying Halo Orbit Amplitudes

Transfers between halo orbits of different amplitudes have been demonstrated by several researchers using a variety of strategies.[30–32] Employing the chart in Fig. 16, candidate halo orbits with a potential for low-cost transfers can be identified. Recall that the halo orbits are represented by more than one line in the chart, indicating that, for a range of Jacobi constant values, more than one halo orbit exists. Energy levels for which two or more distinct halo orbits exist and possess stable/unstable invariant manifolds may admit free transfers between the orbits. Locating the Jacobi constant values on the chart for which more than one L_1 halo orbit exists yields a range of $C = 2.998 - 3.004$ for which three distinct orbits exist. From the range $C = 2.998 - 2.999$, two unstable and one linearly stable halo orbit appear as candidates; from $C = 2.999 - 3.004$, three unstable halo orbits exist. The Jacobi constant values for which two distinct L_2 halo orbits exist is $C = 3.015 - 3.059$; two unstable halo orbits are also available for $C = 3.017 - 3.058$.

To search for a free or low-cost transfer between two L_1 halo orbits of different amplitudes, values of Jacobi constant within the specified ranges are selected, and two distinct halo orbits at this energy level are chosen. The unstable (stable) manifolds associated with the halo orbit possessing the smaller (larger) ratio A_z/A_y are considered. Using methods demonstrated by Haapala and Howell,[33,34] Poincaré maps are employed in the search for a low-cost transfer. Here, a surface of section is selected at an x-coordinate value that lies between the x-axis crossings of the two halo orbits. For example, for the L_1 halo orbits plotted in black in Fig. 20, a value of $x_* = -2.1 \times 10^4$ km (left of the Moon in Moon-centered coordinates) is selected, corresponding to the gray surface $\Sigma = \{\bar{x} | x = x_*\}$. The unstable (stable) manifolds associated with orbits of lower (higher) ratio A_z/A_y are computed, and crossings of Σ are recorded. Each crossing is plotted using a

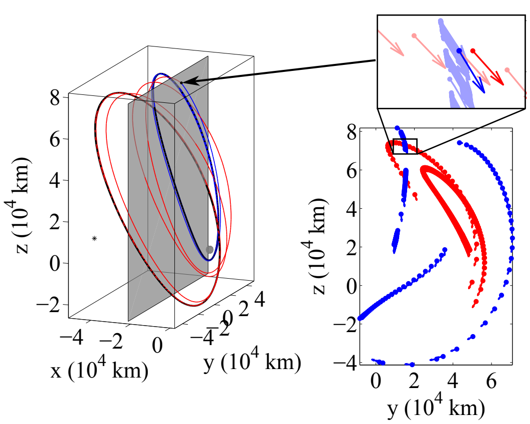

Fig. 20 Employing Poincaré maps to locate an initial guess for the transfer

vector such that the basepoint is defined as (y, z), and the vector components correspond to $k \cdot (\dot{y}, \dot{z})$, where k is a scaling factor. This representation avoids the definition of the additional constraints required to reduce the map dimension in the previous example. Locating nearby vectors with similar length and orientation, and propagating the associated initial conditions, generally offers a suitable initial guess for a low-cost transfer. A corrections algorithm is applied that allows the Jacobi constant value associated with the periodic orbits to vary, as well as the departure/insertion location of the unstable/stable manifold, and the time-of-flight along the manifold arcs. Continuity along the transfer is enforced, with a Δv allowed where the stable and unstable manifolds are linked. Using this process, the sample transfers appearing in Figs. 21-22 are constructed, each requiring $\Delta v = 10$ m/s. The Jacobi

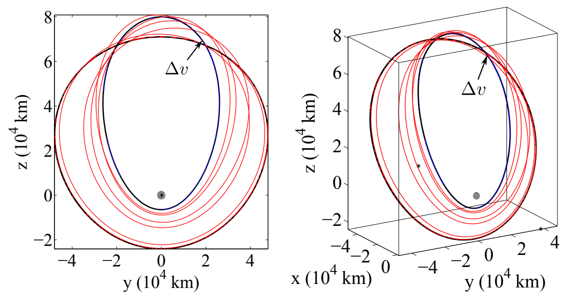

Fig. 21 Shifting between L_1 halo orbits, 75.2 day transfer (66.5 days along red arc), $C_1 = 3.0000$, $C_2 = 3.0040$, $A_z/A_y = 1.48 \rightarrow 3.06$, $\Delta v = 10$ m/s

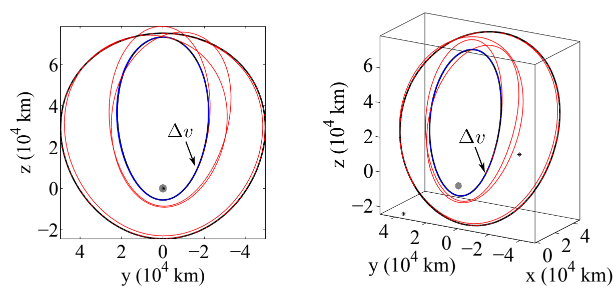

Fig. 22 Shifting between L_2 halo orbits, 71.2 day transfer (45.6 days along red arc), $C_1 = 3.0231$, $C_2 = 3.0348$, $A_z/A_y = 1.52 \rightarrow 3.35$, $\Delta v = 10$ m/s

constant values, C_1 and C_2, for the departure and insertion halo orbits are noted in the figure captions and clearly require a maneuver to compensate, although they do lie within the previously specified ranges. For the corrected transfers, the stable manifold does not depart significantly from the halo orbit. Thus, it may be possible to generate transfers of similar cost for final orbits that do not possess a stable manifold.

Selecting Orbits within Constraint Cones

For many missions, the need to enforce constraints on the amplitude of a libration point orbit may exist. The MAP mission required a Sun-Earth/Moon L_2 Lissajous orbit that avoided the Earth's shadow, resulting in a constraint that the Sun-Earth-vehicle angle remain above 0.5° for the 4-year mission duration.[35] The DSCOVR mission requires an L_1 orbit for which the Earth-spacecraft line-of-sight angle remains between $4-15°$ from the Sun-Earth line for at least 4 years.[36] Such constraints can be incorporated via an overlay of the orbit amplitude information onto a chart such as that in Fig. 17, where orbit amplitudes are given for the Earth-Moon L_2 Lyapunov, vertical, and halo orbits for a range of Jacobi constant values. To demonstrate the application of cone angle constraints during orbit selection, two constraint cones with vertices at the center of the Earth and of half-angles 3° and 6° are arbitrarily selected. In the following example, orbits that maintain the Earth-vehicle angle between $3-6°$ are sought.

To translate the cone angle constraints into amplitude constraints, the radii of the cones at the x-location of L_2 are included in Fig. 17 as the orange (47183 km) and cyan (23527 km) lines. While the orbit amplitudes in the figure do not necessarily correspond to this x-value, it serves as a useful first approximation. From Fig. 17, it is clear that a small range of halo orbits exists for which A_y and A_z are within the $3-6°$ amplitude range. Selecting $C = 3.115$, indicated by a dashed black vertical line in Fig. 17, within this small range yields the green halo orbit, appearing in Fig. 23, that maintains the desired constraints over the entire path. While the selected halo orbit is predicted to possess a nontrivial center manifold ($n_C = 4$), a quasi-halo orbit at this energy level will likely violate the constraints. From the chart, however, a second

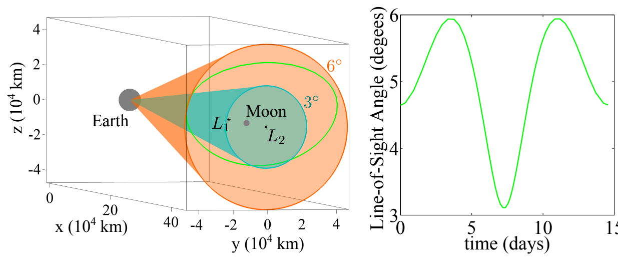

a) Halo orbit ($C = 3.115$) **b)** Angle history

Fig. 23 Halo orbit satisfying cone constraints

option emerges in terms of quasi-Lyapunov or quasi-vertical orbits. There exists a range of C values for which the Lyapunov orbit A_y and vertical orbit A_z lie within the specified amplitude ranges. For example, at $C = 3.135$, an unstable ($n_C = 2$) Lyapunov orbit exists for which A_y is nearly equal to the 6° amplitude, and an unstable ($n_C = 4$) vertical orbit exists with A_z between the $3-6°$ amplitude range. While both periodic orbits cross through $(y, z) = (0, 0)$ and necessarily violate the constraints, a center manifold is expected for the vertical orbit, and Lissajous orbits that meet the constraints over some time period may exist. Sample members from the family of Lissajous tori are computed for $C = 3.135$ and 100 revolutions along the orbits are propagated using states from the invariant circle and a differential corrections process to enforce full-state continuity along each orbit. Examining the tori within the family, a solution is located that lies between the constraint cones for 40.92 days. Increasing the energy level to $C = 3.125$, the Lyapunov orbit A_y violates the 6° amplitude constraint. However, Lissajous orbits still exist that meet the constraints for some time interval. A sample torus and 100 revolution propagation appear in Fig. 24(a) for $C = 3.125$. The portion along the orbit that satisfies

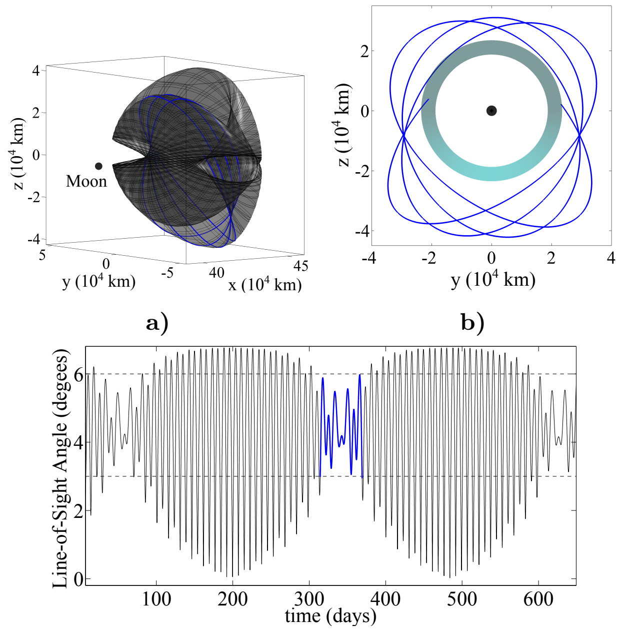

a) b)

c)

Fig. 24 A portion of a Lissajous orbit ($C = 3.125$) meeting cone constraints

the constraints is 54.83 days long and appears in Fig. 24 in blue, with the inner cone in cyan in Fig. 24(b).

Conclusions

Multi-body orbits, such as libration point orbits, have been well studied and a great deal of information is available about their structure and evolution. Exploiting the knowledge about these orbits during the mission design process proves valuable to select orbits that best meet specific mission constraints. Here, a general framework for the global solution space in the vicinity of the libration points is charted, and strategies to display this information are explored. Such guidelines prove useful to evaluate the available periodic and quasi-periodic orbit types and to understand the evolution of the solution space with certain parameters, such as the energy level. A design process that exploits this information about the available orbit structures is demonstrated for sample design scenarios.

Acknowledgments

The authors appreciate the support of NASA Goddard Space Flight Center under Internal Research

And Development (IRAD) grants NNX12AC57G, NNX13AE55G, and NX13AM17G, and of NASA Headquarters: Science Mission Directorate; Planetary Science Division under grant NNX13AH02G. Additional support from the Purdue University Graduate School, the College of Engineering, and the School of Aeronautics and Astronautics is also appreciated.

References

[1] T. A. Bray, and C. L. Goudas, Doubly Symmetric Orbits about the Collinear Lagrangian Points, *Astronautical Journal*, **72**, 202-213, 1967.

[2] R. W. Farquhar, and A. A. Kamel, Quasi-periodic orbits about the translunar libration point, *Celestial Mechanics*, **7**, 458-473, 1973.

[3] J. V. Breakwell, J. V. Brown, The 'halo' family of 3-dimensional periodic orbits in the earth-moon restricted 3-body problem, *Celestestial Mechanics*, **20**, 389-404, 1979.

[4] K. C. Howell, Families of orbits in the vicinity of the collinear libration points, *Journal of the Astronautical Sciences*, **49**, 107-125, 2001.

[5] E. Campbell, *Bifurcations from Families of Periodic Solutions in the Circular Restricted Problem with Application to Trajectory Design*. Ph.D. thesis, School of Aeronautics and Astronautics, Purdue University, West Lafayette, Indiana, 1999.

[6] Á. Jorba, J. Masdemont, Dynamics in the center manifold of the collinear points of the restricted three body problem, *Physica D*, **132**, 189-213, 1999.

[7] G. Gómez, and J. M. Mondelo, The dynamics around the collinear equilibrium points of the RTBP, *Physica D*, **157**, 283-321, 2001.

[8] D. Grebow, *Generating Periodic Orbits in the Circular Restricted Three-Body Problem with Applications to Lunar South Pole Coverage*. M.S. Thesis, School of Aeronautics and Astronautics, Purdue University, West Lafayette, Indiana, 2006.

[9] M. Lo, B. Williams, W. Bollman, D. Han, Y. Hahn, J. Bell, E. Hirst, R. Corwin, P. Hong, K. Howell, B. Barden, and R. Wilson, GENESIS Mission Design, *Journal of the Astronautical Sciences*, **49**, 169-184, 2001.

[10] K. C. Howell, and J. P. Anderson, "Generator's User's Guide, Version 3.0.2," IOM AAE-0140-012, July, 2001.

[11] K. C. Howell, and J. J. Guzmán, "Generator," IOM AAE-0140-010, 2001.

[12] M. Lo, "LTool Version 1.0G Delivery," JPL, IOM 00-2147, September, 2000.

[13] J. M. Mondelo, E. Barrabés, G. Gómez, and M. Ollé, "Numerical Parametrizations of Libration Point Trajectories and their Invariant Manifolds," 23rd AAS/AIAA Space Flight Mechanics Meeting, Kauai, Hawaii, February, 2013. Paper No. AAS 07-321.

[14] E. J. Doedel, and B. E. Oldeman, "AUTO-07P: Continuation and Bifurcation Software for Ordinary Differential Equations," January, 2012.

[15] A. F. Haapala, M. Vaquero, T. A. Pavlak, K. C. Howell, and D. C. Folta, Trajectory Selection Strategy for Tours in the Earth-Moon System, *AAS/AIAA Astrodynamics Specialist Conference*, Hilton Head, South Carolina, August 10-15, 2013. Paper No. AAS 13-782.

[16] D. Folta, N. Bosanac, D. Guzzetti, and K. Howell, An Earth-Moon System Trajectory Design Reference Catalog, *Acta Astronautica*, in press, 2014. DOI http://www.sciencedirect.com/science/article/pii/S0094576514002938

[17] D. Guzzetti, N. Bosanac, and K. C. Howell, A Framework for Efficient Trajectory Comparison in the Earth-Moon Design Space, *AIAA/AAS Astrodynamics Specialist Conference*, San Diego, CA, August 4-7, 2014.

[18] V. Szebehely, *Theory of Orbits: The Restricted Problem of Three Bodies*. Academic Press, New York, United States, 1967.

[19] G. Gómez, M. Marcote, and J. M. Mondelo, The invariant manifold structure of the spatial Hills problem, *Dynamical Systems: An International Journal*, **20**, 115-147, 2005.

[20] R. A. Broucke, Periodic orbits in the restricted three-body problem with Earth-Moon masses, NASA-JPL TR 82-1168, 1968.

[21] E. J. Doedel, R. C. Paffenroth, H. B. Keller, D. J. Dichmann, J. Galán-Vioque, A. Vanderbauwhede, Computation of Periodic Solutions of Conservative Systems with Application to the 3-Body Problem, *International Journal of Bifurcation and Chaos*, **13**, 1353-1381, 2003.

[22] K. C. Howell, and H. J. Pernicka, Numerical Determination of Lissajous Trajectories in the Restricted Three-Body Problem, *Celestial Mechanics*, **41**, 107-124, 1988.

[23] E. Castellá, and Á. Jorba, On the vertical families of two-dimensional tori near the triangular points of the bicircular problem, *Celestial Mechanics and Dynamical Astronomy*, **76**, 35-54, 2000.

[24] E. Kolemen, J. Kasdin, P. Gurfil, Quasi-periodic orbits of the restricted three-body problem made easy, *New Trends in Astrodynamics and Applications III, AIP Conference Proceedings*, **886**, 68-77, Princeton, New Jersey, August 16-18, 2007.

[25] Z. Olikara, and D. Scheeres, Numerical method for computing quasi-periodic orbits and their stability in the restricted three-body problem, *1st IAA/AAS Conference on the Dynamics and Control of Space Systems,* Porto, Portugal, March, 2012.

[26] G. Gómez, A. Jorba, J. Masdemont, and C. Simó, Study of the transfer from the Earth to a halo orbit around the equilibrium point L1, *Celestial Mechanics and Dynamical Astronomy*, **56**, 541-562, 1993.

[27] D. Folta, T. Pavlak, A. Haapala, and K. Howell, Preliminary Considerations for Access and Operations in Earth-Moon L1/L2 Orbits, *23rd AAS/AIAA Space Flight Mechanics Meeting*, Kauai, Hawaii, 2013. Paper No. AAS 13-339.

[28] J. S. Parker, and G. H. Born, Direct lunar halo orbit transfers, *The Journal of the Astronautical Sciences*, **56**, 441-476, 2008.

[29] G. Gómez, W. S. Koon, M. W. Lo, and J. E. Marsden, Connecting orbits and invariant manifolds in the spatial restricted three-body problem, *Nonlinearity*, **17**, 1571-1606, 2004.

[30] L. A. Hiday-Johnston, and K. C. Howell, Transfers Between Libration-Point Orbits in the Elliptic Restricted Problem, *Celestial Mechanics and Dynamical Astronomy*, **58**, 317-337, 1994.

[31] G. Gómez, Á. Jorba, and C. Simó, Study of the Transfer Between Halo Orbits, *Acta Astronautica*, **43**, 493-520, 1998.

[32] K. E. Davis, R. L. Anderson, D. J. Scheeres, and G. H. Born, Locally Optimal Transfers Between Libration Point Orbits Using Invariant Manifolds, *19th AAS/AIAA Space Flight Mechanics Meeting*, Savannah, Georgia, 2009. Paper No. AAS 09-398.

[33] A. F. Haapala, and K. C. Howell, Trajectory design strategies applied to temporary comet capture including Poincaré maps and invariant manifolds, *Celestial Mechanics and Dynamical Astronomy*, **116**, 299-323, 2013.

[34] A. F. Haapala, and K. C. Howell, Representations of Higher-Dimensional Poincaré Maps with Application to Spacecraft Trajectory Design, *Acta Astronautica*, **96**, 23-41, 2014.

[35] A.Edery, Earth Shadows and the SEV Angle of MAP's Lissajous Orbit At L2, , *AIAA/AAS Astrodynamics Specialist Conference*, Monterey, California, 2002. Paper No. AIAA 2002-4428.

[36] T. Pavlak, *Trajectory Design and Orbit Maintenance Strategies in Multi-Body Dynamical Regimes*. M.S. Thesis, School of Aeronautics and Astronautics, Purdue University, West Lafayette, Indiana, 2013.